

Table S1. CMIP6 experiments and models used in this study.

Experiment	Description	Model
historical	CMIP6 historical simulation	CMCC-ESM2, ACCESS-CM2, ACCESS-ESM1-5, AWI-CM-1-1-MR, AWI-ESM-1-1-LR, BCC-CSM2-MR, BCC-ESM1, CAMS-CSM1-0, CanESM5, CanESM5-1, CAS-ESM2-0, CESM2, CESM2-WACCM, CMCC-CM2-HR4, CMCC-CM2-SR5, CMCC-ESM2, FGOALS-g3, FIO-ESM-2-0, GISS-E2-1-G, GISS-E2-1-H, GISS-E2-2-G, GISS-E2-2-H, IITM-ESM, MCM-UA-1-0, MIROC6, MPI-ESM-1-2-HAM, MPI-ESM1-2-HR, MPI-ESM1-2-LR, MRI-ESM2-0, NESM3, NorCPM1, NorESM2-LM, NorESM2-MM, SAM0-UNICON, TaiESM1
hist-aer	Anthropogenic-aerosol-only historical simulations	
hist-GHG	Well-mixed greenhouse-gas-only historical simulations	CanESM5, MRI-ESM2-0, BCC-CSM2-MR, CESM2, FGOALS-g3, MIROC6, GISS-E2-1-G
hist-nat	Natural-only historical simulations (solar irradiance, stratospheric aerosol)	
hist-CO ₂	CO ₂ -only historical simulations	MIROC6, CanESM5
ssp245-aer	Extension of at least one hist-aer simulation through the 21 st century using SSP2-4.5 tropospheric aerosol concentrations/emissions	NorESM2-LM, MIROC6, CanESM5
ssp245-GHG	Extension of at least one hist-GHG simulation through the 21 st century using the SSP2-4.5 greenhouse gas concentrations	CanESM5, GISS-E2-1-G, IPSL-CM6A-LR, MIROC6, NorESM2-LM
ssp119	Carbon neutral scenario	CanESM5-1, CanESM5, GFDL-ESM4, FGOALS-g3, IPSL-CM6A-LR, MIROC6, MPI-ESM1-2-LR, MRI-ESM2-0
ssp126	Low emission scenario	CESM2-WACCM, TaiESM1, MRI-ESM2-0, MIROC6, KACE-1-0-G, IPSL-CM6A-LR, INM-CM5-0, INM-CM4-8, GFDL-ESM4, FGOALS-f3-L, CMCC-ESM2, CAS-ESM2-0, CanESM5, CanESM5-1, BCC-CSM2-MR, ACCESS-ESM1-5, ACCESS-CM2, CMCC-CM2-SR5
ssp245	Medium emissions scenario	
ssp370	Medium to high emissions scenario	
ssp585	High emission scenario	

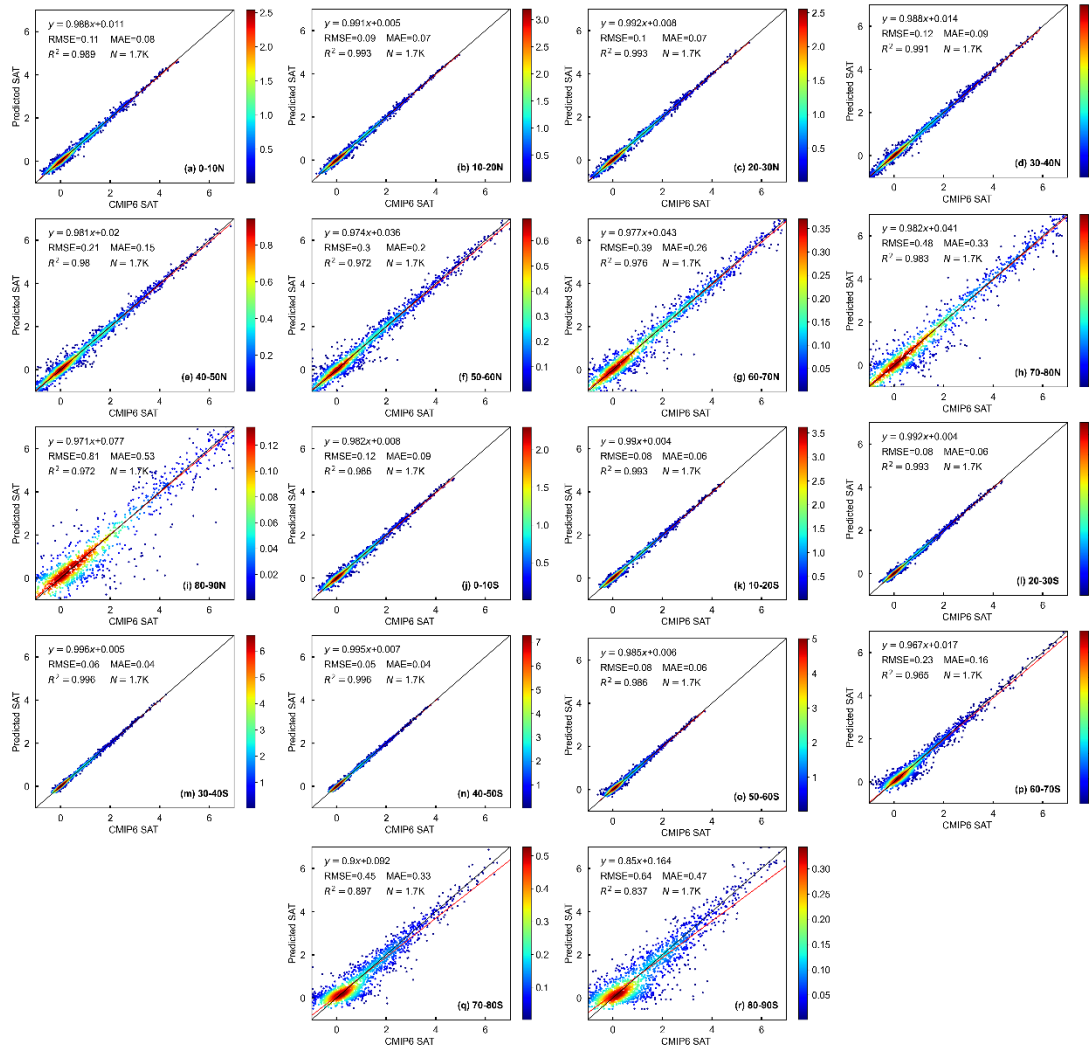


Figure S1. Scatterplot of the SAT density ($^{\circ}\text{C}$) from CMIP6 multimodel simulations versus the predicted values from the LightGBM model for the eighteen latitudinal bands each spacing 10° from 90°S to 90°N , with color bars indicating the density of the data distribution. The black and red solid lines are the 1:1 lines and linear regression lines, respectively. Statistical metrics including RMSE, MAE, and R^2 are given in the upper left corner of each panel.

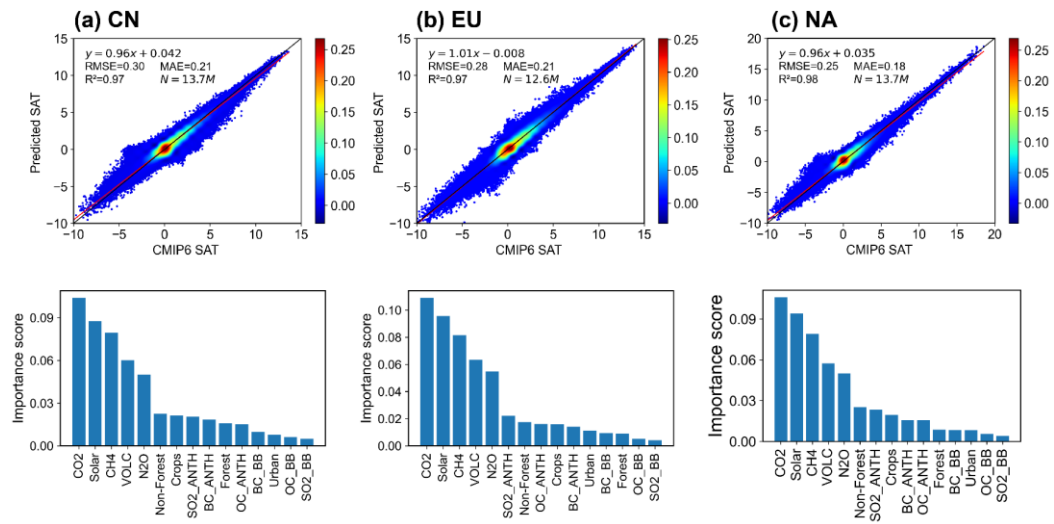


Figure S2. Scatterplot of the SAT density (°C) (top) and importance scores for the input variables (bottom) of the three regional LightGBM models for (a) China, (b) Europe and (c) North America.

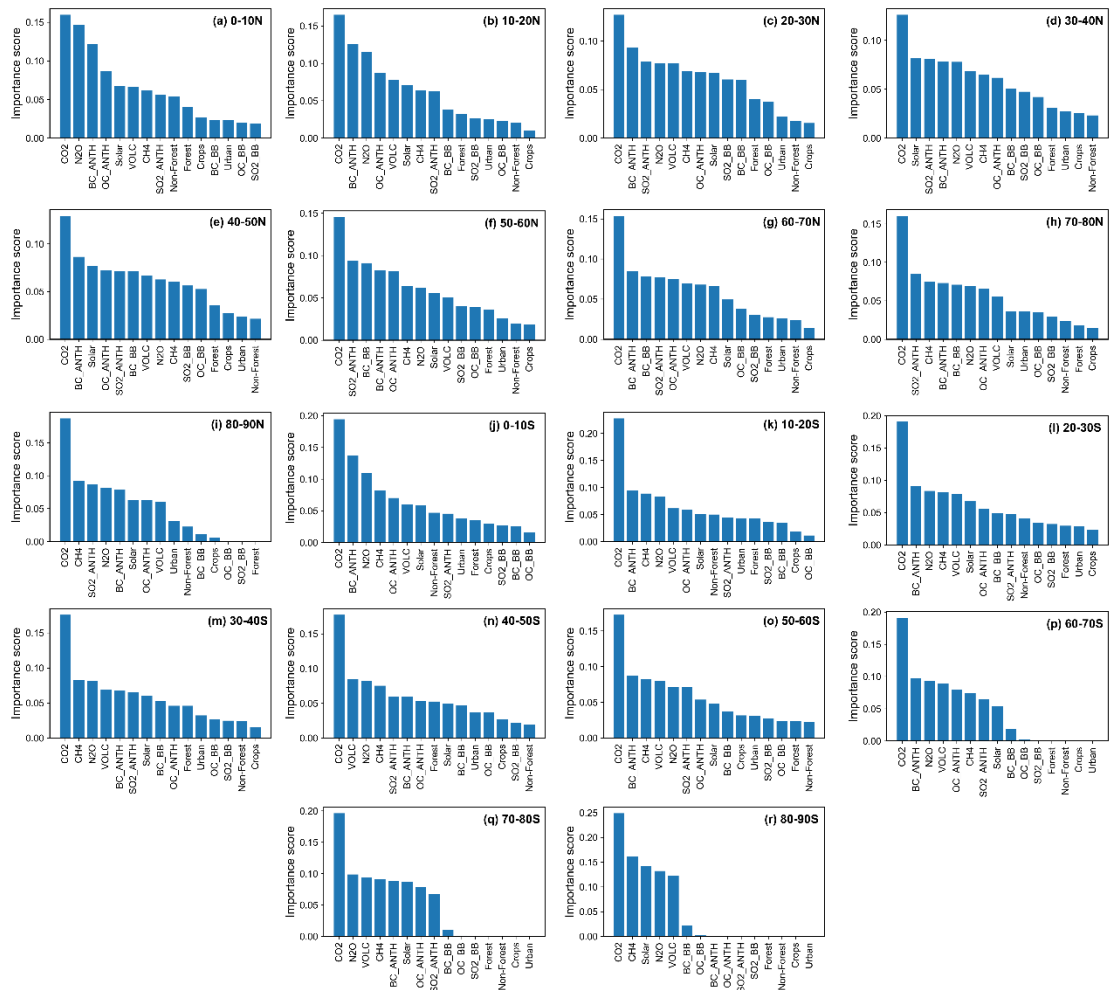


Figure S3. Importance scores for the input variables (aerosols, GHGs, land use, solar radiation and volcanic forcing) of the eighteen LightGBM models for the 18 latitudinal bands.

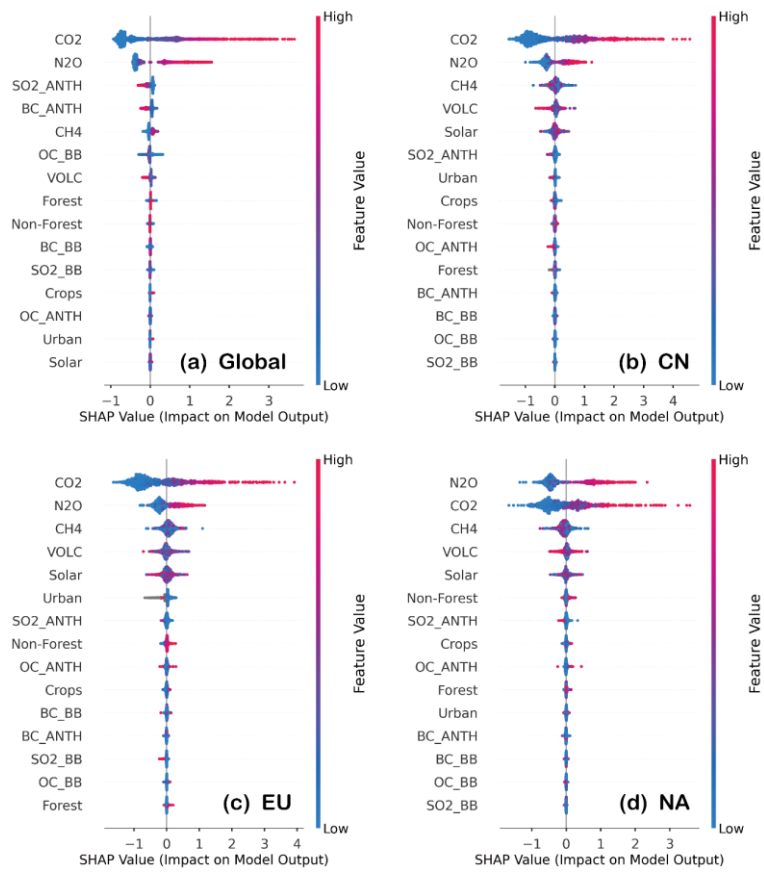


Figure S4. Shapley Additive Explanations (SHAP) values of LightGBM models for predicting (a) global and regional SAT over (b) China, (c) Europe, and (d) North America.

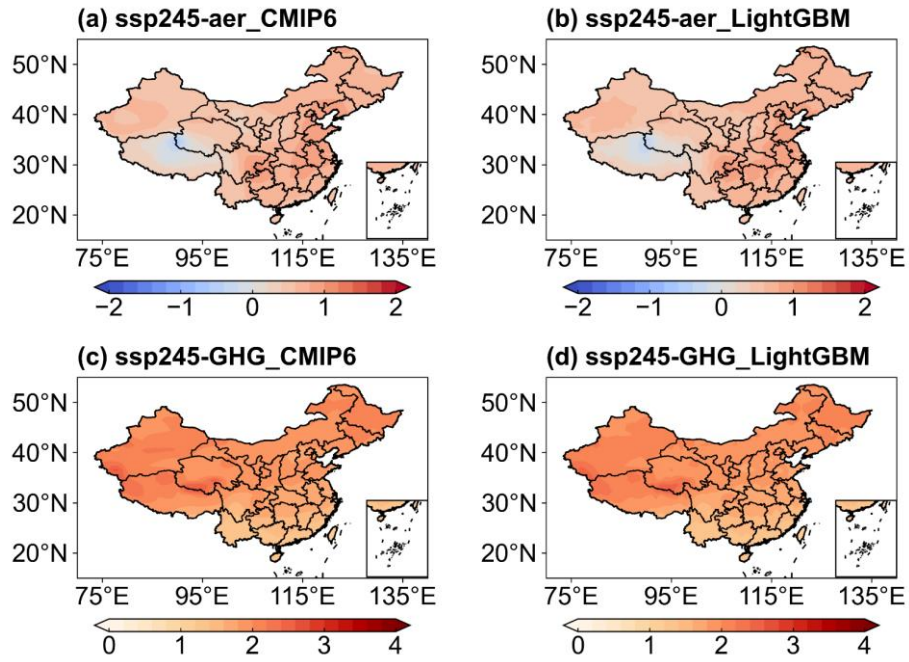


Figure S5. Changes in SAT ($^{\circ}\text{C}$) in China in 2095 (2091-2100 average) relative to 2020 (2015-2024 average) due to (a, b) anthropogenic aerosol and (c, d) GHG changes in CMIP6 multi-model simulations (left) and LightGBM projections (right) in the SSP2-4.5 scenario.

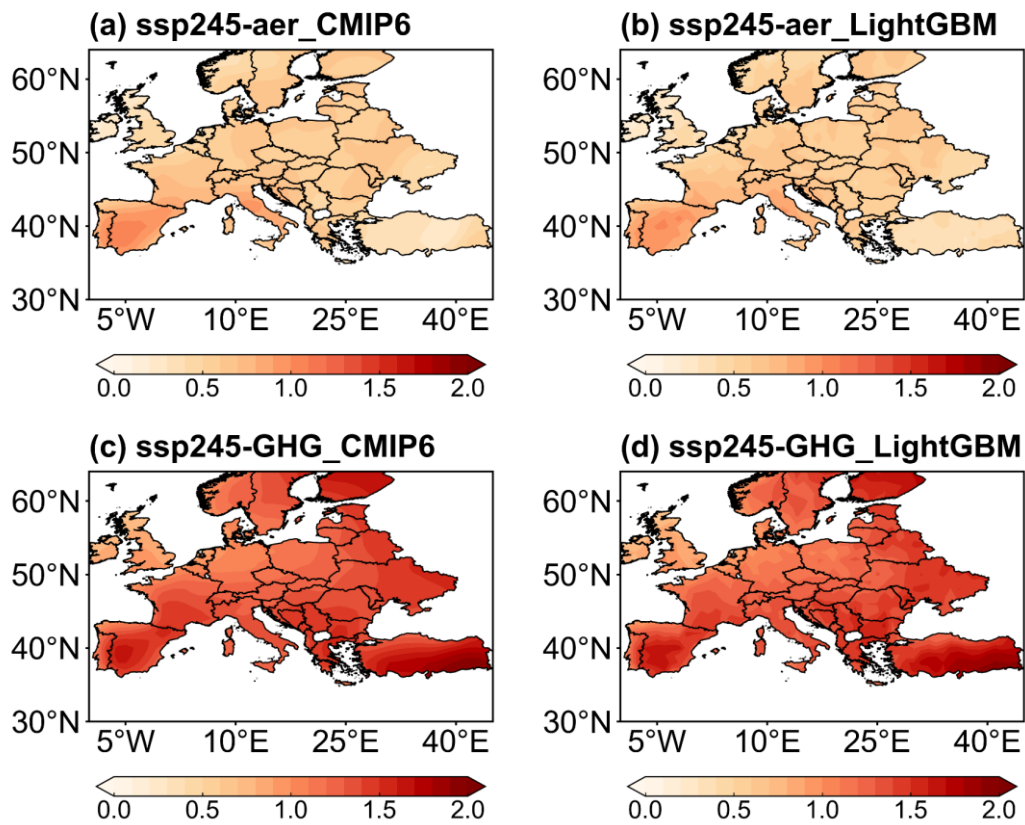


Figure S6. Same as Fig.S5, but for Europe.

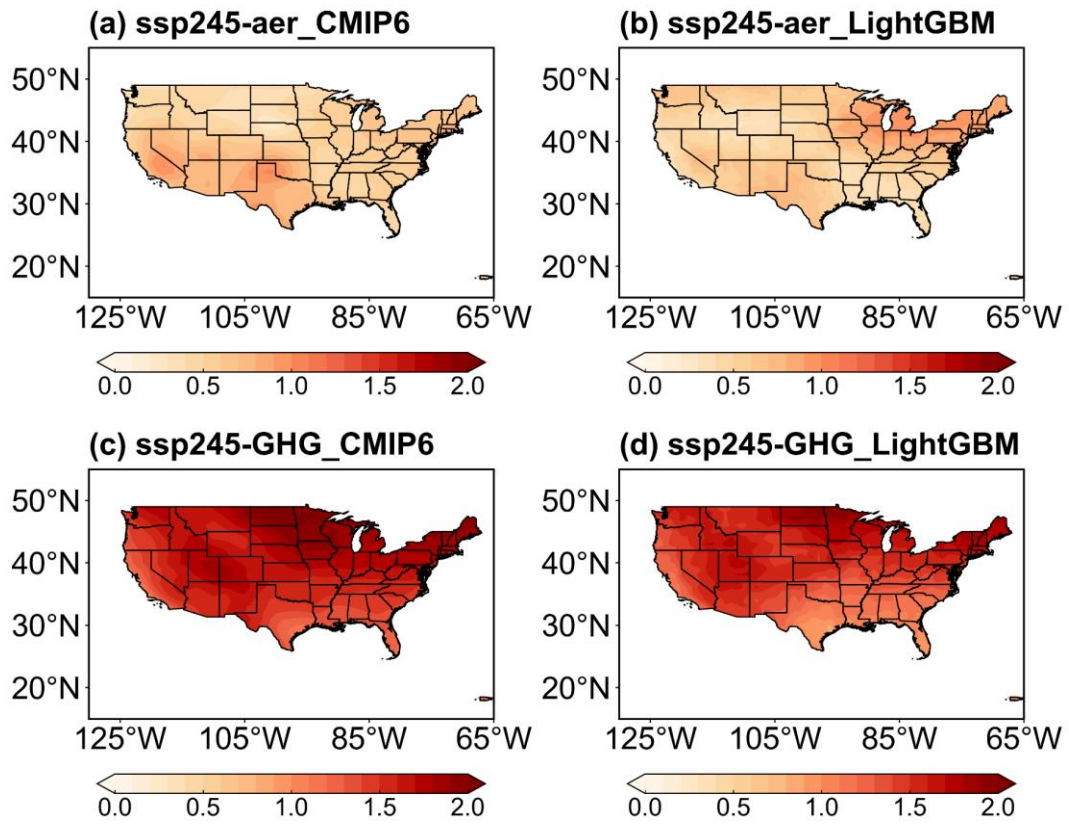


Figure S7. Same as Fig.S5, but for North America.

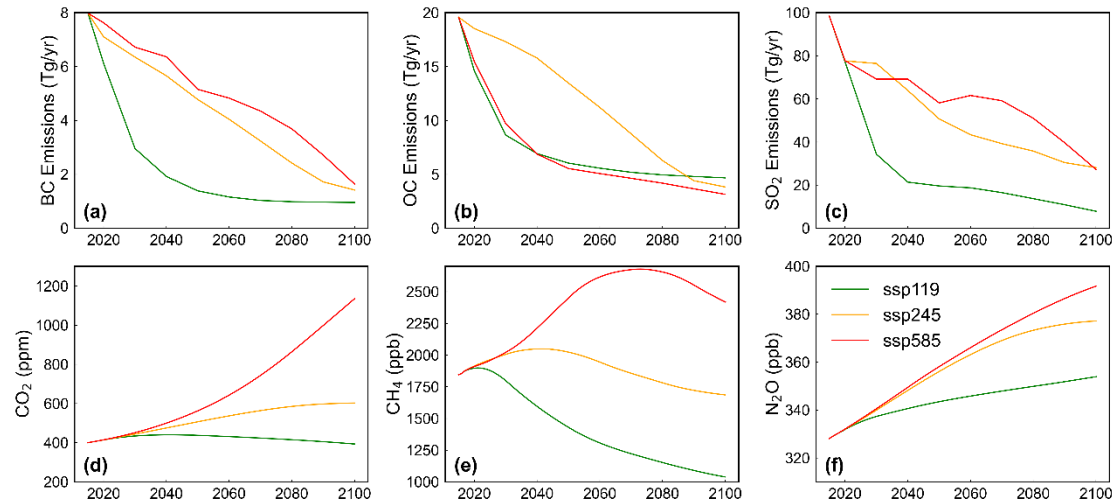


Figure S8. Time series of future variations in global anthropogenic emissions of aerosols or precursors (BC, unit: Tg C/yr, OC, unit: Tg C/yr, and SO₂, unit: Tg SO₂/yr) and GHGs concentrations (CO₂, unit: ppm, CH₄, unit: ppb and N₂O, unit: ppb).

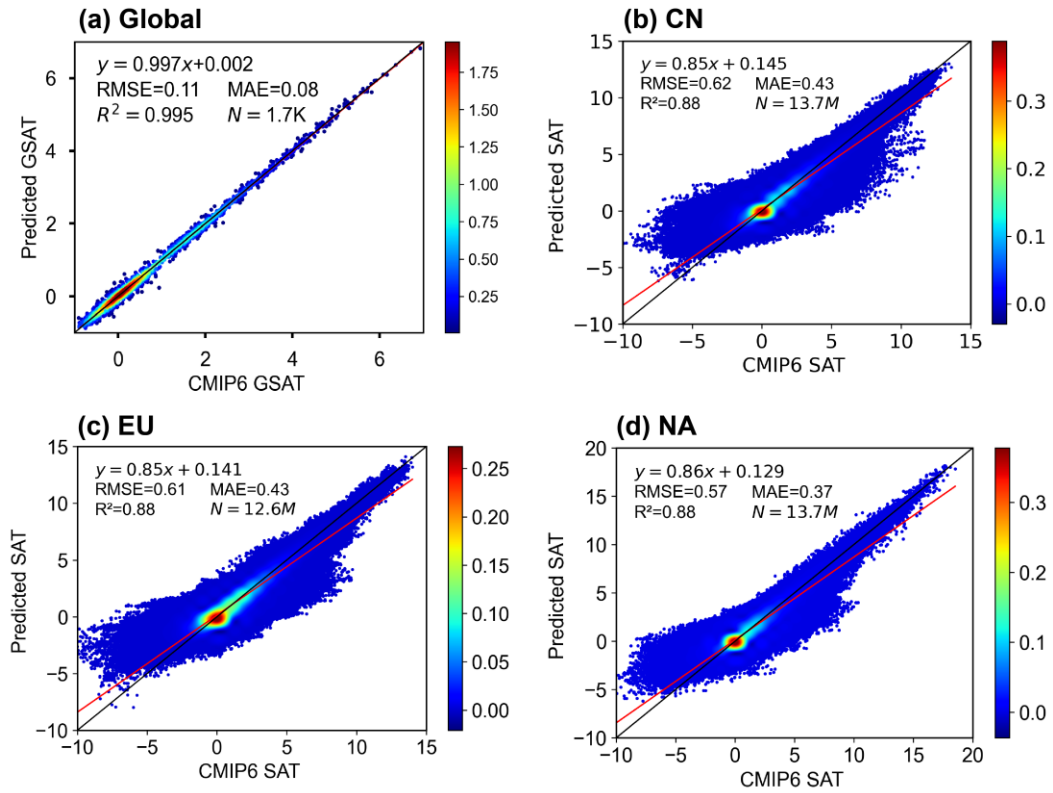


Figure S9. Scatterplot of the SAT density ($^{\circ}C$) of the XGBoost models for (a) Global, (b) China, (c) Europe, and (d) North America.

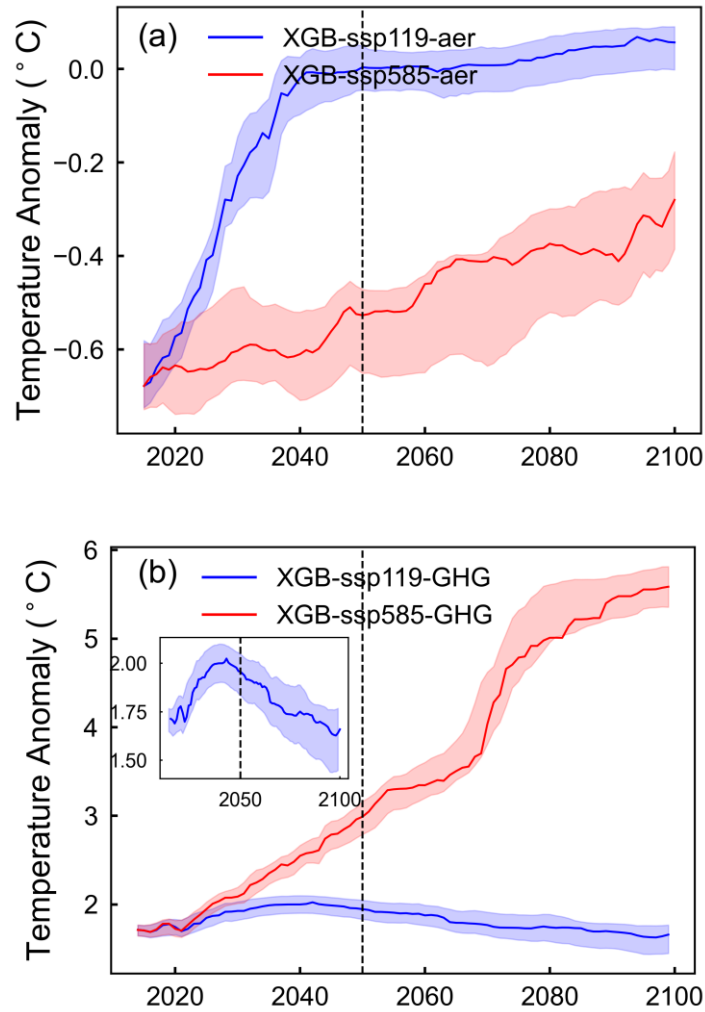


Figure S10. Time series of XGBoost-predicted GSAT anomalies (°C) during 2015–2100 under the SSP1-1.9 and SSP5-8.5 due to changes in (a) anthropogenic aerosols and (b) GHGs. The inner figure in (b) is the GSAT anomalies due to changes in GHGs under the SSP1-1.9 scenario. Shaded areas indicate the range of the ML prediction by random separation of training and testing datasets for 100 times.

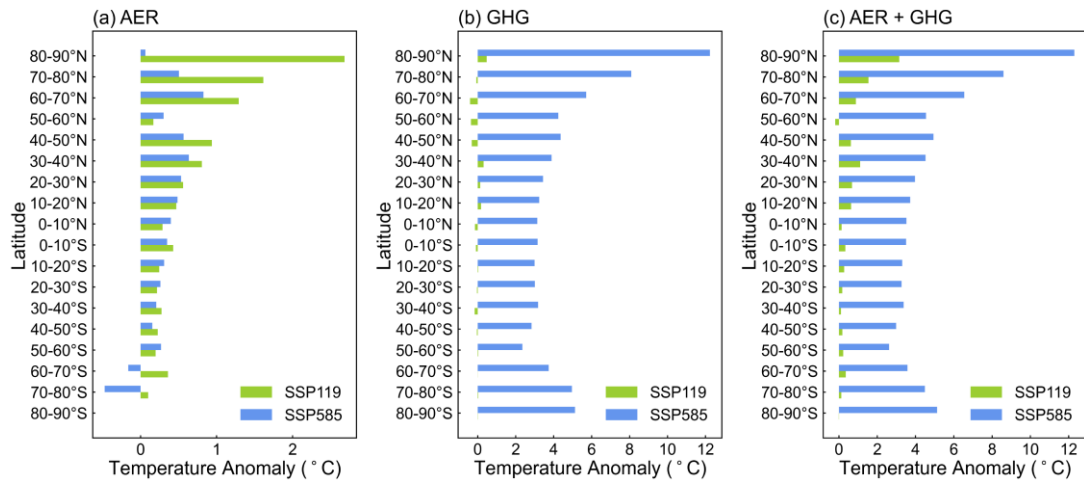


Figure S11. Attribution of changes in SAT (°C) in each 10° latitudinal band from 90°S to 90°N to future changes in (a) anthropogenic aerosols, (b) GHGs and (c) both of them in 2095 (averaged 2091–2100) relative to 2020 (averaged over 2015–2024) under the SSP1-1.9 and SSP5-8.5 scenarios predicted by the XGBoost models.

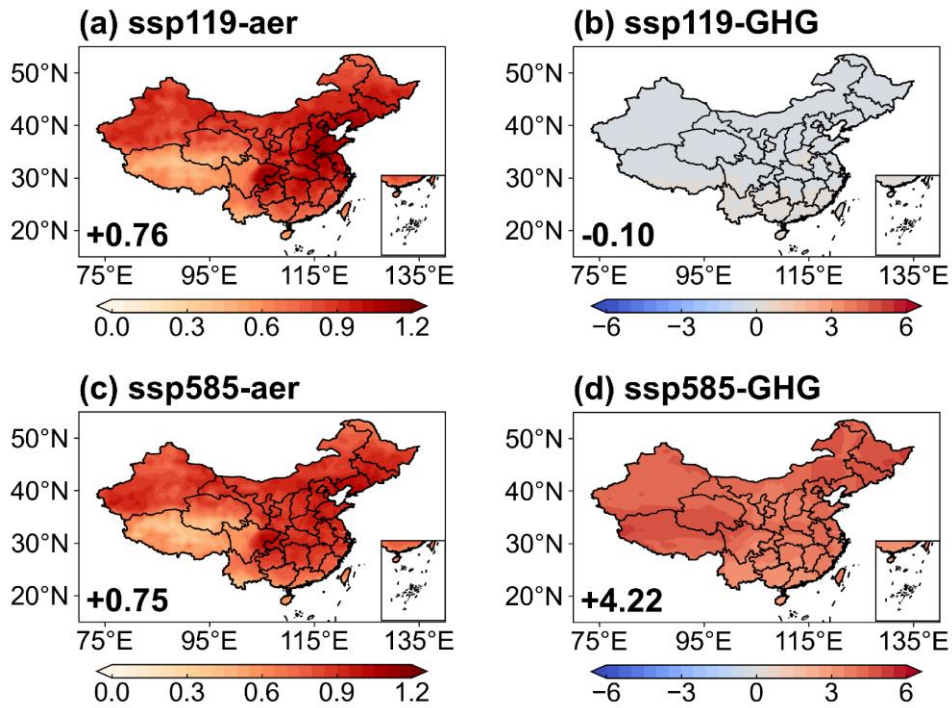


Figure S12. Attribution of changes in SAT (°C) in China to future changes in anthropogenic (a, c) aerosols and (b, d) GHGs in 2095 (averaged 2091–2100) relative to 2020 (averaged over 2015–2024) under the SSP1-1.9 and SSP5-8.5 predicted by the XGBoost models. The regional averages are shown in the bottom left of each panel.

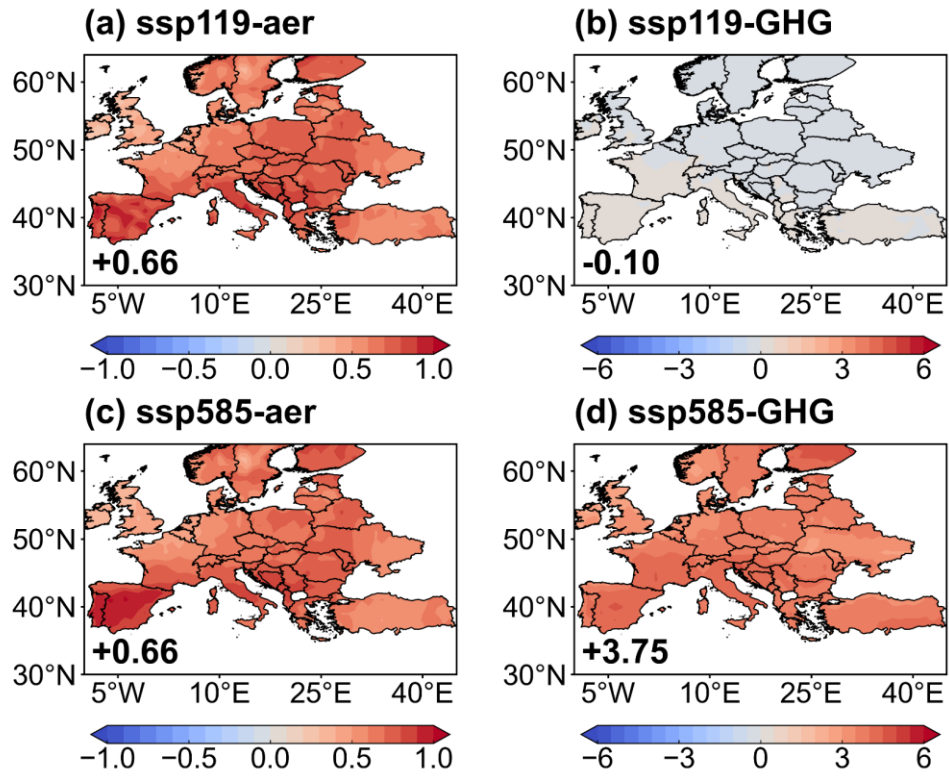


Figure S13. Same as Fig. S12, but for Europe.

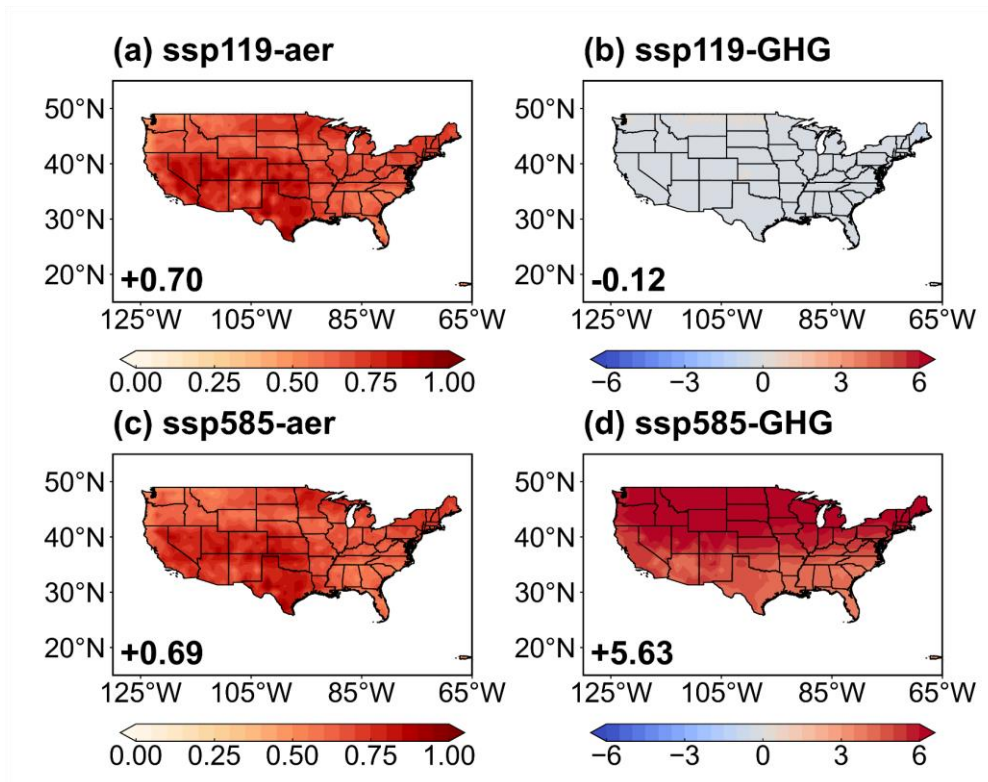


Figure S14. Same as Fig.S12, but for North America.